



Ironmaking & Steelmaking

Processes, Products and Applications

ISSN: (Print) (Online) Journal homepage: <https://www.tandfonline.com/loi/yirs20>

Electrolysis of iron with oxygen gas evolution from molten sodium borate electrolytes

Ho-Gil Choi , Seungwoo Choi , Min-Kyung Kim , Juyoung Jang , Ki Tae Nam , In-Ho Jung & Kyung-Woo Yi

To cite this article: Ho-Gil Choi , Seungwoo Choi , Min-Kyung Kim , Juyoung Jang , Ki Tae Nam , In-Ho Jung & Kyung-Woo Yi (2021): Electrolysis of iron with oxygen gas evolution from molten sodium borate electrolytes, Ironmaking & Steelmaking, DOI: [10.1080/03019233.2020.1861837](https://doi.org/10.1080/03019233.2020.1861837)

To link to this article: <https://doi.org/10.1080/03019233.2020.1861837>



Published online: 11 Jan 2021.



Submit your article to this journal [↗](#)



Article views: 2



View related articles [↗](#)





View Crossmark data [↗](#)

RESEARCH ARTICLE



Electrolysis of iron with oxygen gas evolution from molten sodium borate electrolytes

Ho-Gil Choi^a, Seungwoo Choi^a, Min-Kyung Kim^a, Juyoung Jang^{a,b}, Ki Tae Nam ^a, In-Ho Jung^a and Kyung-Woo Yi ^a

^aDepartment of Materials Science and Engineering, Seoul National University, Seoul, Korea; ^bCenter for Energy Materials and Technology (KIST), Seoul, Korea

ABSTRACT

Molten oxide electrolysis can be used to reduce the carbon dioxide emissions from ironmaking. In this paper, we electrochemically decompose iron oxide (Fe_2O_3) into iron (Fe) and oxygen (O_2) using boron trioxide and sodium oxide ($\text{B}_2\text{O}_3\text{-Na}_2\text{O}$) as the molten oxide electrolyte at 1000°C that is less than the temperature of other molten oxide electrolysis. The formation of Fe at the cathode and O_2 at the anode is identified by analysing products from both electrodes. The results suggest that the cathodic current efficiency of electrolysis at 2 V is about 54.7%, energy consumption is about $5.27 \text{ kW h kg}^{-1}$ of Fe at 2 V electrolysis, and purity of the reduced Fe was more than 97 mol.%. With respect to the process temperature and product yield, $\text{B}_2\text{O}_3\text{-Na}_2\text{O}$ molten oxide has potential as a supporting electrolyte to reduce Fe_2O_3 to Fe without consuming any carbon.

ARTICLE HISTORY

Received 19 June 2020
Revised 5 November 2020
Accepted 6 December 2020

KEYWORDS

Molten oxide electrolysis; carbon-free ironmaking process; metal extraction; oxygen evolution; sodium borate; high current efficiency; low energy consumption; thermogravimetric analysis

Introduction

For every ton of steel produced, 1.83 tons of carbon dioxide (CO_2) is emitted. For the steelmaking industry overall, roughly three billion tons of CO_2 is emitted annually [1]. To reduce CO_2 emissions, technology development is ongoing in the steelmaking industry, such as blast furnace with top gas recycling, hydrogen-based reduction, carbon capture utilisation and storage, biomass application, and electrolysis [2,3]. Electrolysis is an innovative technology with the potential to significantly reduce CO_2 emissions [4]. In essence, iron ore is reduced using electricity as a reducing agent and oxygen (O_2) is emitted as a by-product with an inert anode; producing the iron (Fe) does not consume any carbon, theoretically. Moreover, CO_2 emissions can be further reduced using electricity from carbon neutral sources, such as nuclear power, solar photovoltaics, and wind turbines.

The electrolysis of iron oxide (Fe_2O_3) has been studied in the laboratory with various electrolytes, such as aqueous solution [5], molten hydroxide [6], molten carbonate [7], molten salt [8], and molten oxide [9–12]. As an aqueous electrolyte, sodium hydroxide is advantageous because it can result in Fe electrolysis at low temperatures (110°C) with minimal electronic current losses; however, it is also disadvantageous insofar that solubility to the feedstock is low, and the hydrogen evolving reaction takes place in competition with the Fe reduction reaction, which means that the current efficiency is low [5]. Alternatively, chlorides have high electrical conductivity and are often used as electrolytes in electrowinning and electrorrefining. They are disadvantageous insofar as the solubility of oxygen ions is low for oxide electrolysis [13]. On the other hand, the oxide feedstock is highly soluble in the molten oxide, and current density is high due to the

high concentration of ions in the electrolyte [14]. The feedstock can be electrolysed by feeding raw material into the electrolyte without any additional processes [15]. One of the major problems concerning oxide electrolysis is that the acidic oxide forms a network structure that deteriorates the mass transfer characteristics, including viscosity. This can be overcome by adjusting the basicity of the oxide [16]. The process of reducing Fe using silicon dioxide, magnesium oxide, calcium oxide, and aluminium oxide ($\text{SiO}_2\text{-MgO-CaO-Al}_2\text{O}_3$) as a supporting electrolyte achieves a high current density (1 A cm^{-2} and greater) and produces highly pure Fe [9]; however, high temperatures are required.

The aim of the present study is to produce Fe without consuming carbon using molten oxide electrolysis at a temperature that is less than other molten oxide electrolysis. With an inert anode, O_2 gases are evolved as a by-product while Fe_2O_3 is reduced by the electricity, which means that Fe is produced without emitting CO_2 gas. A molten oxide with a high solubility to various oxides is used as an electrolyte. It is advantageous in terms of current density as well as the removal of gangue from the reduced Fe when iron ore is used as the feedstock. Moreover, the oxide electrolyte used in the present study is molten at temperatures less than 1000°C .

Experimental

Boron oxide (B_2O_3) powder, sodium peroxide (Na_2O_2) granules (Alfa Aesar), and Fe_2O_3 powder were manually mixed at a room temperature. The mixture was placed in an alumina crucible (44 mm in diameter), which was placed in an electrolytic furnace with air. The furnace was heated to 1050°C , which was maintained for 1 h to obtain sodium oxide (Na_2O) by decomposing Na_2O_2 and stabilise the

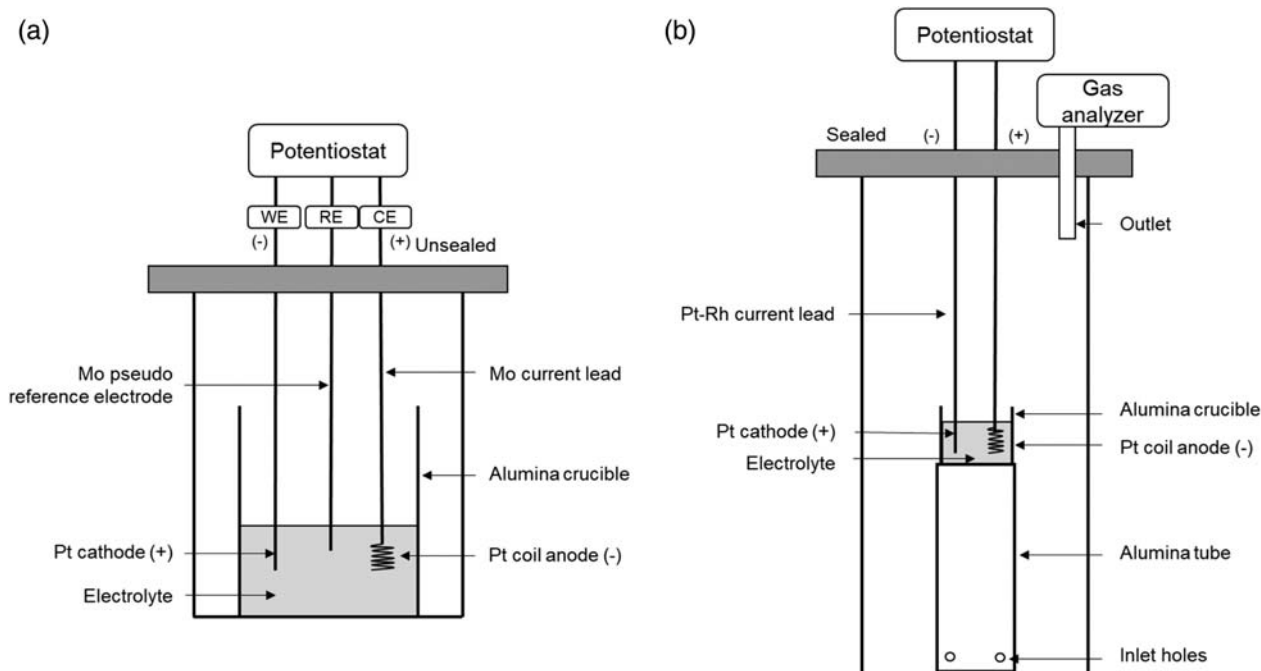


Figure 1. Schematic diagrams of electrolytic cells (not to scale) (a) for analysing the cathode reactions, electrolysis, and (b) for analysing the outlet gas.

electrolyte. A platinum (Pt) wire (0.5 mm in diameter) and Fe wire (0.5 mm in diameter) were used as the working electrode, a coil (5 mm in diameter) made from Pt wire (0.5 mm in diameter) was used as the counter electrode, and a molybdenum (Mo) wire (5 mm in diameter) was used as the reference electrode. These electrodes were connected to Mo wires (0.5 mm in diameter), which served as the current leads. The alumina tube covered the Mo wires.

Figure 1 shows schematic diagrams of electrolytic cells. For analysing the cathode reactions and producing Fe, the electrolytic cell in Figure 1(a) was used. The alumina crucible containing oxide mixture was placed in the electrolytic furnace unsealed. The furnace temperature was controlled at 1050°C for the temperature of the electrolyte to be 1000°C. The type B thermocouple was used to measure the temperature of the electrolyte. A Pt wire and a Pt coil were connected to each Mo current lead. The current leads were connected to a potentiostat (CHI 600E, CH Instruments). The electrolytic cell in Figure 1(b) was used to measure the anodic product. An alumina crucible (70 mm in diameter) was sealed in an alumina tube (100 mm in diameter and 930 mm in height) with highly pure argon (Ar) gas (99.999%) flowing at a rate of 200 mL min⁻¹. O₂ Concentration of outlet gas was measured by a gas analyser (Rapidox 3100, Cambridge Sensotec). Pt–Rh wires (0.5 mm in diameter) were used as current leads, which were shrouded by the alumina tubes.

Electrochemical experiments were conducted using a B₂O₃–Na₂O electrolyte (70 and 30 mol.%, respectively). Components of the electrolyte were selected in terms of the melting temperature, solubility to Fe₂O₃, and electrical conductivity. B₂O₃ satisfies conditions of low melting temperature with sufficient solubility to Fe₂O₃. Furthermore, the oxide mixture with the addition of Na₂O becomes suitable for an electrolyte in the liquid phase since Na₂O breaks a network structure of molten B₂O₃. Experiments consisted of three-electrode cyclic voltammetry (CV) measurements and constant voltage electrolysis. The depth of the working electrode immersed in the electrolyte was measured to calculate the surface area. To obtain the electrodeposited iron,

constant voltage electrolysis with the two electrodes was performed. After the electrolysis, the electrodes were lifted, separated from the electrolyte, and cooled. The electrode deposit at the cathode was analysed using X-ray diffraction (XRD, D8 Advance, Bruker), optical microscopy (OM, DFC420, Leica), scanning electron microscopy (SEM, SU70, Hitachi), and energy dispersive X-ray spectroscopy (EDS, SU70, Hitachi).

The amount of reduced Fe from electrolysis was analysed by thermogravimetric analysis (TGA, SDT Q600, TA Instruments). Figure 2 shows the preparation steps for TGA. After electrolysis, the cathode was separated from the electrolyte and cooled in air, after which the attached material at the cathode (A) was recovered. A was grinded into powder (B) and a magnet was used to further select powder for the TGA (C) from B. The total amount of selected powder was divided into some samples. The TGA experiments were conducted using these samples. The temperature was maintained at 150°C for 2 h (first step), after which it was raised to 900°C at a rate of 10°C min⁻¹ (second step) and maintained at said temperature for 3 h with O₂ gas flowing (third step). During this process, the weight change of the sample was measured.

Results and discussion

Electrolyte selection

The melting point of B₂O₃ is 450°C, which is low for an oxide and it can dissolve Fe₂O₃ at 1000°C up to 50 wt.%; however, B₂O₃ is unsuitable for an electrolyte due to the network forming property in the liquid phase. According to previous studies, the addition of a basic oxide to an acidic oxide melt increases the optical basicity [17], decreases the kinematic viscosity, increases the limiting current density [16], and increases the electrical conductivity [18]. Accordingly, Na₂O was added as the supporting electrolyte, thereby creating the B₂O₃–Na₂O mixture.

Figure 3(a) shows the binary phase diagram of the B₂O₃–Na₂O system at 1 atm. The oxide mixture becomes the molten state at 1000°C in the entire composition range

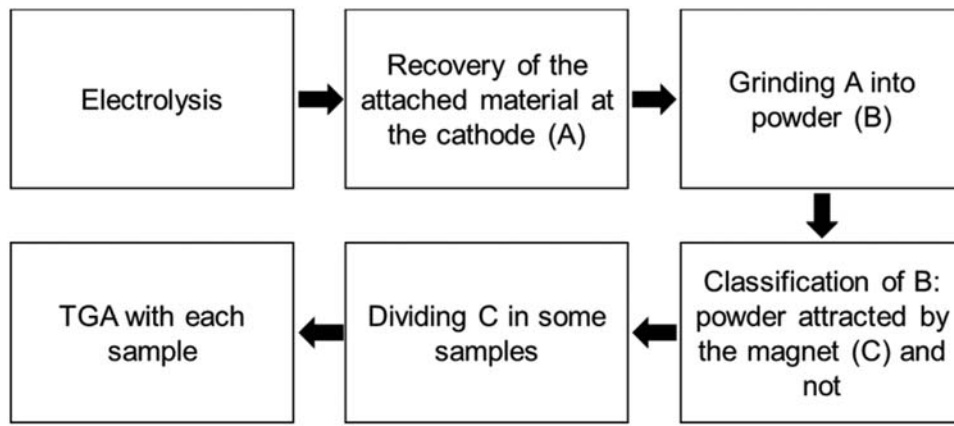


Figure 2. Preparing samples for TGA.

except Na_2O -rich region. As mentioned above, increasing the basicity of oxide melt improves the transport properties of the molten oxide electrolyte. Accordingly, an electrolyte with a high Na_2O concentration is optimal for electrolysis with respect to transport properties. However, according to a previous study using an iridium (Ir) anode, anode stability is reduced in a basic melt compared with an acidic one [10]. Since Pt is used as an anode material in the present study, a composition with Na_2O less than 50 mol-% is suitable for a supporting electrolyte. Especially, the eutectic composition of 70 mol-% B_2O_3 and 30 mol-% Na_2O was selected in this study to take advantage of its low melting temperature. Composition and properties of the selected electrolyte at the experimental condition are summarised in Table 1. Physico-chemical properties are evaluated from FactSage 7.3 version (melting temperature and viscosity) and previous studies (density [19] and conductivity [20]). Figure 3(b) shows the isopleth of (70 mol-% B_2O_3 + 30 mol-% Na_2O) – Fe_2O_3 in the ternary B_2O_3 – Na_2O – Fe_2O_3 system in air [21]. According to the diagram, the maximum solubility of Fe_2O_3 in the melt with 70 mol-% B_2O_3 and 30 mol-% Na_2O is 9.94 mol-%.

Electrochemical analysis

Figure 4(a) shows the cyclic voltammograms of the Pt-wire working electrode with the Mo-wire pseudo-reference

electrode in molten oxide electrolyte with and without Fe_2O_3 . In the curve of the Pt working electrode in the supporting electrolyte (dashed-dotted line), reduction current increased continuously from roughly -0.3 V. This increase appears as the supporting electrolyte decomposes. During the anodic scan, the onset of the oxidation current is observed at 1.1 V with some fluctuations. This behaviour is observed when the gas evolving reaction occurred at the anode, which is consistent with the CV results of an Ir anode reported by Wang et al. [9]. Because the electrolyte is oxide and the Pt electrode is inert, the gas produced by the oxidation reaction is O_2 . When 5 wt-% Fe_2O_3 is added to the supporting electrolyte, reduction peaks are observed at -0.13 (R1), 0.09 (R2), and 0.32 V (R3) as well as oxidation peaks at 0.04 (O1) and 0.55 V (O3) (solid line). It is likely that the O1 and O3 peaks are the anodic counterparts of the R1 and R3 peaks, respectively. The oxidation peak counterpart to the R2 peak is covered by the O1 or O3 peak. As these peaks are absent in the voltammogram of the supporting electrolyte, they originate from the redox reactions of the added Fe ions. To identify the reaction at the R2 peak, CV was conducted with the Fe cathode. The curve of the Fe working electrode in the supporting electrolyte has a different pattern from that of the Pt working electrode, as shown in Figure 4(b). A reduction peak is observed, and the Fe electrode dissolves at the backward scan (solid line).

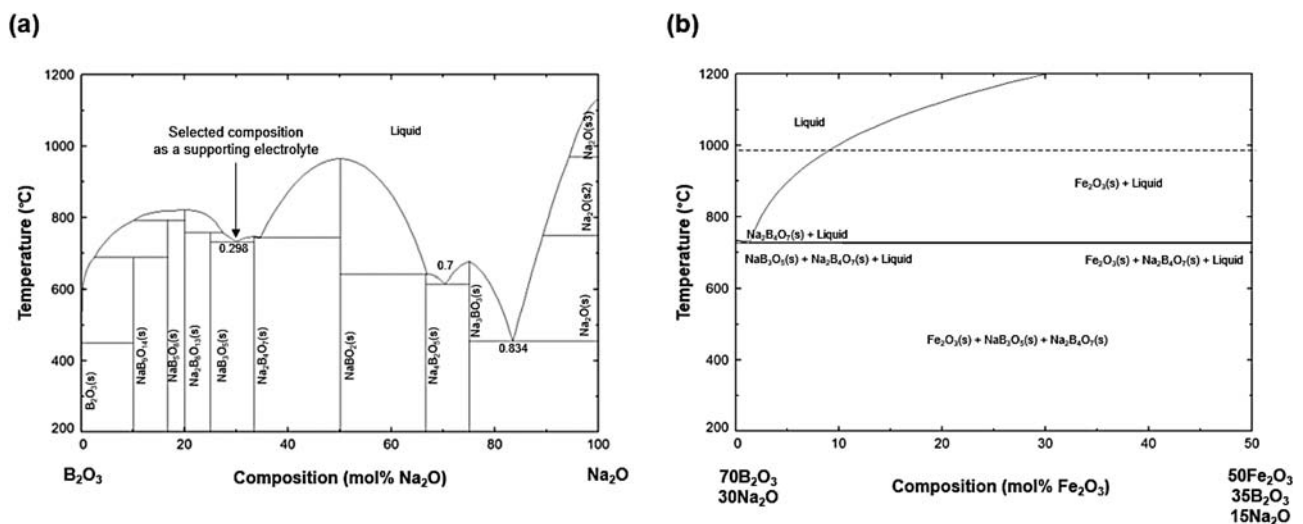


Figure 3. (a) Binary phase diagram of B_2O_3 – Na_2O at 1 atm with an O_2 partial pressure of 0.21. (b) Vertical section of ternary phase diagram of the B_2O_3 – Na_2O – Fe_2O_3 system under the same pressure condition. The diagrams are calculated from FactSage 7.3 version with FTOD database [21].

Table 1. Composition (mol-%) and properties of the selected electrolyte at the experimental condition.

B ₂ O ₃	Na ₂ O	T _m (°C)	Viscosity (Pa s)	Density (g cm ⁻³)	Conductivity (S cm ⁻¹)
70	30	732.6	~0.15	~1.99	~1.08

Considering that the current was almost zero when the Pt wire was used as a working electrode in the supporting electrolyte, the increase in the reduction and oxidation current can be attributed to the redox reaction of the Fe electrode. The R2 peak shown in the voltammogram of the Pt working electrode (Figure 4(a)) was not observed in that of the Fe working electrode. In the binary system of Pt and Fe, both form solid solutions [22], and, because the activity of reduced metal in the alloy is less than unity, the reduction potential of the alloy is more positive than that of pure metal. Accordingly, the R2 peak can be attributed to the reduction of Fe by forming an alloy with Pt on the surface of the electrode.

Figure 5 shows the cyclic voltammograms obtained by changing the scan rate of the electrolyte containing 1 wt-% Fe₂O₃. The peak potential (E_p) and half peak potential ($E_{p/2}$) were measured along with the scan rate to investigate the number of electrons transferred at each peak. The diagnostic criteria of the voltammograms are outlined below [23,24].

Reversible reaction with a soluble product:

$$E_{p/2} - E_p = 2.2 \frac{RT}{nF}. \quad (1)$$

Reversible deposition of metals on the solid electrode:

$$E_{p/2} - E_p = 0.7725 \frac{RT}{nF}, \quad (2)$$

where n is the number of the electrons transferred in the reaction and F is the Faraday constant. Table 2 shows the $E_{p/2} - E_p$ and n values calculated using each equation. For the R1 peak, E_p shifted in the less cathodic direction and $E_{p/2} - E_p$ decreased with a decrease in the scan rate. When the scan rate was lower than 10 mV s⁻¹, the E_p barely changed, which means that the reaction at the R1 peak is reversible when the scan rate decreases. The n values from Equation (2), assuming that metal is deposited reversibly on the solid

electrode, increased as the scan rate decreased and approached a value of two. On the other hand, the n values from Equation (1) assuming a reaction is reversible with soluble product were 5.48 and 5.61 at 5 and 10 mV s⁻¹, respectively. It is hard to assign a reaction to these electrons. From the above results, the reaction at the R1 peak consists of metal deposition with two electrons being transferred. Since the peak occurred when Fe₂O₃ was added to the electrolyte, the resultant reaction is a reduction of Fe from Fe²⁺.

For the R3 peak, E_p was almost constant regardless of the scan rate, and the reaction, therefore, is a reversible system. The n values from Equation (1) were between 1.22 and 1.28; from Equation (2), they ranged between 0.43 and 0.45, which is an irrational number in an electrochemical reaction. Considering the above results, the reaction at the R3 peak is a one-electron reaction, the reduced species of which are soluble in the electrolyte. Since the peak occurred when Fe₂O₃ was added to the electrolyte, the resultant reaction is a reduction of Fe²⁺ from Fe³⁺.

Cathodic product analysis

The electrodeposits obtained by electrolysis were analysed by EDS. Figure 6(a) shows the SEM image and EDS maps of the sample obtained from two-electrode electrolysis at 1.4 V. The electrodeposits had two forms: thin layer on the electrode surface and particles dispersed in the oxide around the electrode. An Fe layer with a thickness of roughly 35 μm was observed around the electrode. Pt was also observed in the Fe region electrodeposited on the electrode surface, which means that an alloy layer is formed when Fe reduction occurs on the Pt electrode. Iron was also observed with particles in the vicinity of the cathode. Figure 6(c) shows the OM image of the 1.4-V electrodeposit. In the image with the long depth of field, it is evident that the Fe observed in the vicinity of the cathode has a dendrite structure. Figure 6(b) shows the SEM images and EDS maps of the sample obtained from two-electrode electrolysis at 2 V, from which it is evident that the electrodeposit has a microstructure similar to that of 1.4 V; however, even though the same charge passed during electrolysis, the two electrodeposits have differences in the thickness of the Fe layer on the

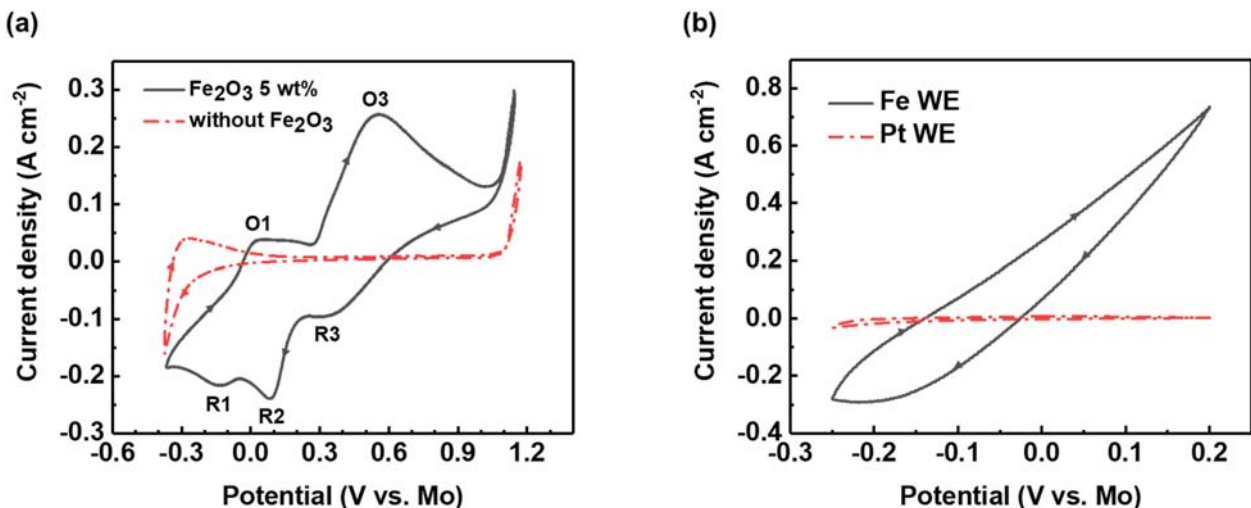


Figure 4. (a) Cyclic voltammograms of a Pt-wire working electrode with a Mo-wire pseudo-reference electrode in B₂O₃-Na₂O without Fe₂O₃ (dashed-dotted line) and with 5 wt-% Fe₂O₃ (solid line) at 1000°C with a scan rate of 100 mV s⁻¹. (b) A cyclic voltammogram of a Fe-wire working electrode with a Mo-wire pseudo-reference electrode in B₂O₃-Na₂O at 1000°C with a scan rate of 50 mV s⁻¹.

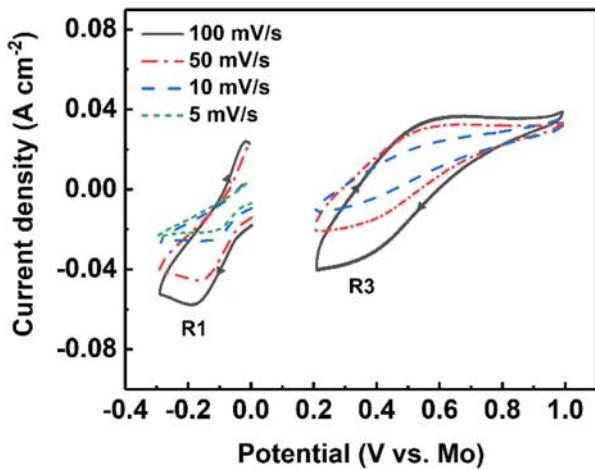


Figure 5. Cyclic voltammograms of a Pt-wire working electrode with a Mo-wire pseudo-reference electrode in B_2O_3 (70 mol-%)- Na_2O (30 mol-%) with 1 wt-% Fe_2O_3 at $1000^\circ C$ with various scan rates: 100 mV s^{-1} (solid line), 50 mV s^{-1} (dashed-dotted line), 10 mV s^{-1} (dashed line), and 5 mV s^{-1} (short dashed line).

surface of the electrode as well as the degree of dendritic growth. In the OM image of the 2-V sample in Figure 6(d), the dendrites have thinner branches than the 1.4-V sample. In addition, the particles that show the cross section of the dendrite branches are also more widespread in the SEM image of the 2-V sample than that of the 1.4-V sample. This dendritic growth can be observed in the mass transport controlled region, the degree of which is consistent with the overpotential applied to the cathode [25].

The TGA experiments were conducted to measure the amount of reduced Fe from 1.4-V electrolysis. The total amount of selected powder was 46.70 mg, which was divided into two samples: C1 (22.01 mg) and C2 (24.69 mg). During the TGA, the weight change of C1 was measured (Figure 7(a)). At the first step, the weight of the powder

converged to a single value; the weight change was 0.01% of the initial powder weight, which can mainly be attributed to the removal of moisture. Most of the weight changes were observed at the second step; the weight of the powder was saturated at the third step. The increase in weight observed during heating can be attributed to the oxidation of Fe in the sample. Thermodynamically, Fe_2O_3 is the most stable phase of Fe (and its oxides) under $1456^\circ C$ at 1 atm of O_2 . The oxidation reaction of Fe and iron(II) oxide can occur for the entire temperature range of TGA. Therefore, the discussed weight change is likely to be involved in both Fe and iron(II) oxide.

The XRD pattern of the attached material before TGA is shown in Figure 7(b). Broad peaks of the amorphous electrolyte and Fe peaks can be observed. Based on the XRD results, no Fe_3O_4 peaks were observed in the XRD pattern of the electrodeposit. We considered the amount of Fe_3O_4 negligible in the samples, and the increase in powder weight from the TGA results can be attributed to the oxidation of Fe. Calculation of current efficiency from a measurement of the weight of reduced Fe by TGA was summarised in Table 3. During the second and third steps, the measured weight change was 4.34 mg. As Fe oxidises to Fe_2O_3 during the TGA, the amount of Fe was 10.09 mg ($(2 \times 55.845)/(3 \times 15.999) \times 4.34\text{ mg}$) in the C1 sample. For C2, the weight change was 4.16 mg. With the same calculations, for C2, the weight of Fe was 9.68 mg, which means that the total Fe was 19.77 mg. Figure 8(a) shows the current according to time during 1.4 V electrolysis, from which it is evident that the amount of total charges was 318 C for 8336 s. As the electrochemical equivalent of Fe is $1.9293 \times 10^{-4}\text{ g}$, the theoretical quantity of electrodeposition is 61.35 mg. The current efficiency of the Fe reduction reaction is calculated by comparing the amount of Fe from the TGA with the theoretical quantity of Fe from the amount of charges recorded on the potentiostat during electrolysis. According to this calculation, the current efficiency is 32.2% at 1.4 V. Additional TGA was also conducted with some of the powder attracted by the magnet obtained from the electrodeposit of 2 V electrolysis. A weight change of 3.01 mg was obtained from the initial weight of 20.32 mg. Using the same calculation as above, the amount of Fe in the sample was 7.00 mg. As the weight of the whole powder attracted by magnet was 97.71 mg, the proportional weight of Fe in said powder was 33.67 mg. As shown in Figure 8(b), the amount of total charges was also 318 C for 1469 s. The theoretical quantity of

Table 2. Cathodic peak potential E_p and n values at R1 and R3 at various scan rates.

Peak	Scan rate (mV s^{-1})	E_p (V)	$E_{p/2} - E_p$ (V)	n from Equation (1)	n from Equation (2)
R1	5	-0.107	0.044	5.48	1.93
	10	-0.112	0.043	5.61	1.97
	50	-0.145	0.060	4.02	1.41
	100	-0.164	0.071	3.40	1.19
R3	10	0.362	0.198	1.22	0.43
	50	0.362	0.193	1.25	0.44
	100	0.355	0.189	1.28	0.45

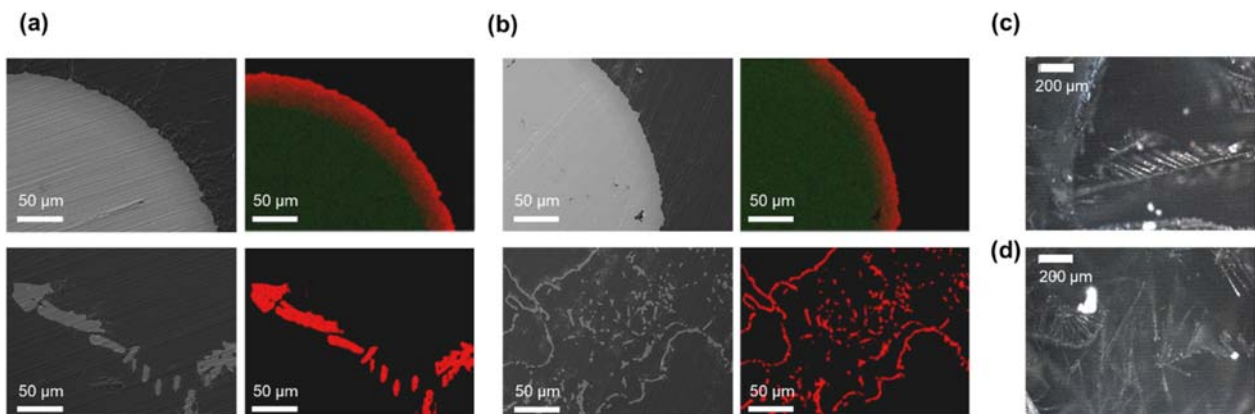


Figure 6. SEM and EDS observations of electrodeposited cross sections from electrolysis at (a) 1.4 and (b) 2 V, and OM images at (c) 1.4 and (d) 2 V.

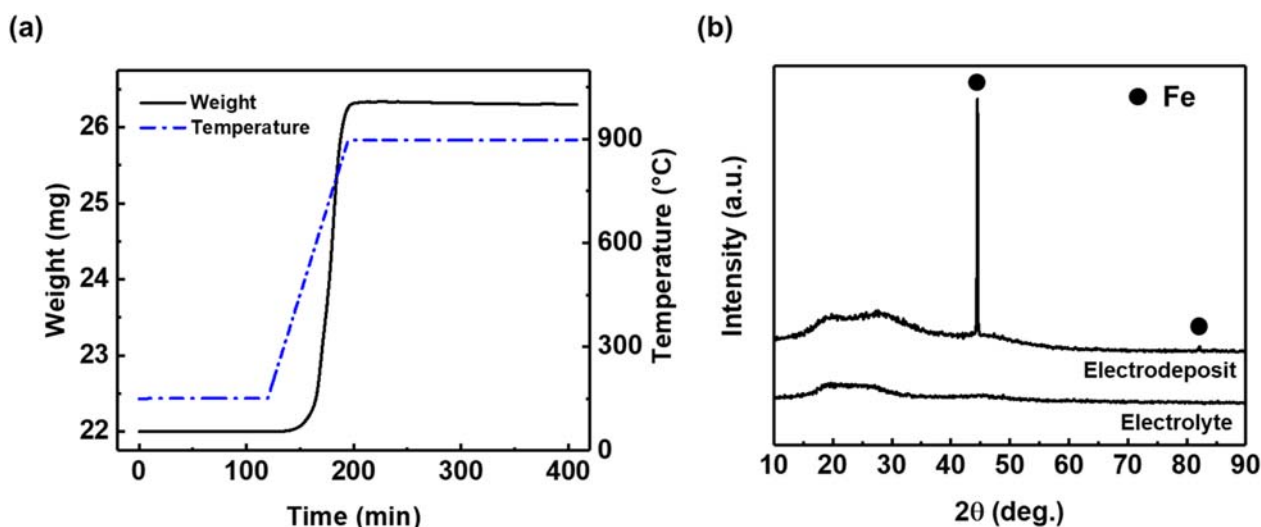


Figure 7. (a) Weight change of electrodeposit at 1.4 V during TGA. (b) XRD pattern of cathodic electrodeposit.

electrodeposition is 61.35 mg since the total charge passed during 2 V electrolysis is the same as that during 1.4 V electrolysis. From the same calculation above, the current efficiency was 54.9% at 2 V. In repeated experiments, the averages of the current efficiencies were 33.2 (± 2.9)% at 1.4 V, and 54.7 (± 2.4)% at 2 V.

Current efficiency of the proposed method

The charge used to reduce Fe_2O_3 to Fe at 1.4 V consisted of 33.2% of the charge passed during electrolysis; the remaining

66.8% corresponds to current loss. Electronic current is a factor in current loss. Electron hopping between ferric and ferrous ions causes electrons to conduct through the electrolyte [26]. In doing so, current flows without Faradaic reactions. Therefore, the electronic current is considered as a factor which lowers the current efficiency of the electrolytic system in the present study.

Stepped potential chronoamperometry was used to quantify the electronic current in the electrolyte system. The long-time values of current correspond to electronic current if Faradaic reaction does not occur [18]. Long-time values of current density were measured along with cell voltage. With the values obtained below a cell voltage of 0.6 V (Figure 9(a)), a linearly extrapolated line was fitted. The linear relation was used to predict the contribution of electronic current at the cell voltage where Faradaic reaction takes place (Figure 9(b)). This prediction was based on the assumption that electronic conductance follows Ohm's law [27]. The electronic current density calculated by the relation was 0.17 A cm^{-2} at 1.4 V, corresponding to 30.4% of the cathode current density of 0.56 A cm^{-2} for 1.4 V electrolysis. Thus, the electronic current is responsible for the efficiency loss of 30.4% for 1.4 V electrolysis. This current efficiency

Table 3. Calculation of current efficiency from a measurement of the weight of reduced Fe from the electrolysis of 1.4 V by TGA.

Weight change of C1 during the TGA (mg)	4.34
Moles of O absorbed in C1 (mol)	2.71×10^{-4}
Moles of oxidised Fe in C1 (mol)	1.81×10^{-4}
Weight of Fe in C1 (mg)	10.09
Weight change of C2 during the TGA (mg)	4.16
Weight of Fe in C2 (mg)	9.68
Weight of Fe in the total sample (mg)	19.77
Total charges (C)	318
Electrochemical equivalent of Fe (g)	1.9293×10^{-4}
Theoretical quantity of electrodeposition (mg)	61.35
Current efficiency (%)	32.2

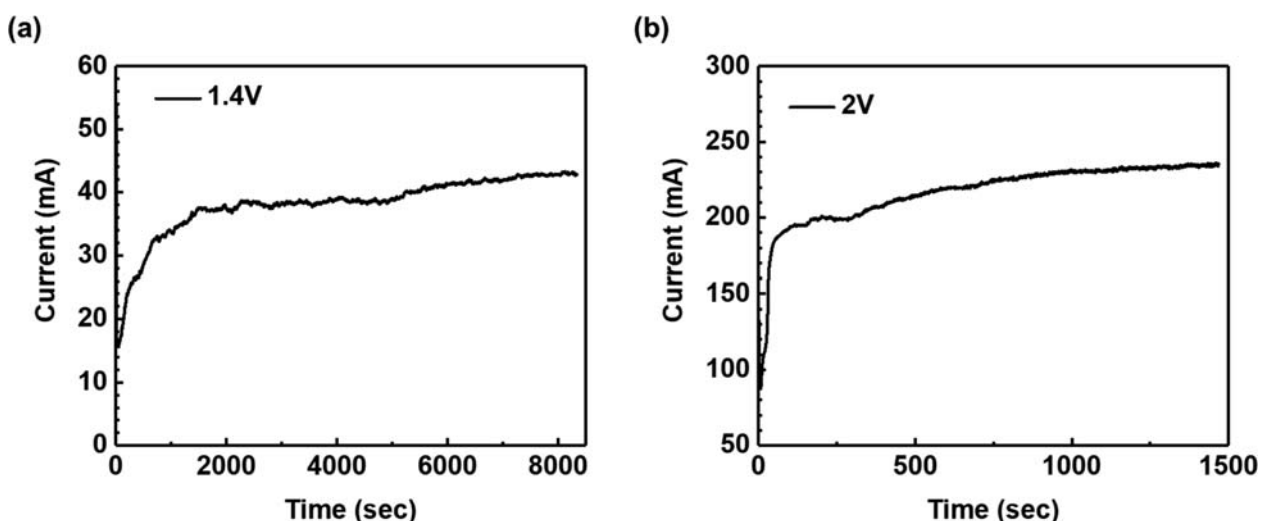


Figure 8. Current variations according to time for electrolysis at (a) 1.4 and (b) 2 V.

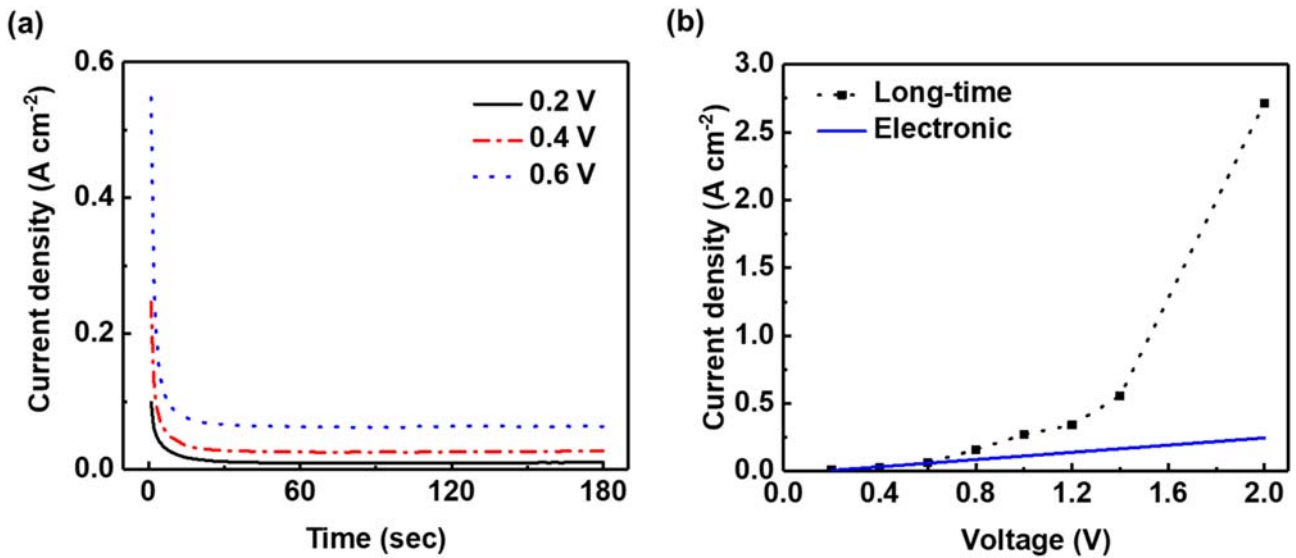


Figure 9. (a) Current decay curves depending on cell voltage. (b) Long-time current densities depending on cell voltage, and linearly extrapolated line of electronic current density fitted by the values of current densities below 0.6 V.

loss can be reduced as the cell voltage increases. The ratio of electronic current to total current decreases as cell voltage increases, as shown in Figure 9(b). The electronic current density at 2 V is 0.25 A cm⁻², which corresponds to 9.2% of the cathode current density of 2.71 A cm⁻². The ratio of electronic current to total current decreased from 30.4% to 9.2% as the cell voltage increased from 1.4 to 2 V. The current efficiencies obtained by TGA are 33.2% and 54.7% at 1.4 and 2 V, respectively. Indeed, the increase in current efficiency between 1.4 and 2 V can be attributed to the decrease in the ratio of electronic current to total current along with an increase in cell voltage.

Energy consumption and reduction of CO₂ emission

The energy consumptions were calculated as follows:

$$E = \frac{VnF}{3600A_{\text{Fe}}\eta}, \quad (3)$$

where E is the energy consumption (kW h kg⁻¹ of Fe), V is the cell voltage, A_{Fe} is the molar mass of Fe, and η is the current efficiency. The values obtained at each electrolysis were summarised in Table 4. The average of the energy consumption was 6.11 (±0.51) kW h 1 kg⁻¹ of Fe at 1.4-V electrolysis. This value contains the energy directly used as electricity during the electrolysis. At 2-V electrolysis, the average of the energy consumption was 5.27 (±0.23) kW h 1 kg⁻¹ of Fe. While increase in the cell voltage contributes to increase in the value of the energy consumption, increase in the cathodic current efficiency contributes reversely.

Oxidation reactions at the anode can occur by free oxide anions (O²⁻) and Fe²⁺ ions. Fe²⁺ ions are formed by the reduction reaction from Fe³⁺ ions at the cathode. Re-oxidation of Fe²⁺ ions at the anode which are reduced at the cathode

leads to current efficiency loss though reduced Fe is formed at the cathode. Figure 10 shows the changes in O₂ concentration of the outlet gas during the 2-V electrolysis. Before beginning electrolysis, the concentration of O₂ in the outlet gas of the electrolytic furnace was measured. Voltage was applied for 3826 s. About 1 min after starting electrolysis, the O₂ concentration measured on the gas analyser increased. The bell-shaped curve represents the measured O₂ concentration, which increases during electrolysis and decreases sharply after the voltage application stopped. It demonstrates that oxygen gas can be evolved as by-product at the anode though current loss by oxidation of Fe²⁺ ions could be included. The obtained results show that the B₂O₃-Na₂O oxide system can produce reduced Fe without CO₂ emission.

The consumption of the anode material should be considered in order to sustain decomposing Fe₂O₃ with oxygen gas evolution. Noble metal anodes such as Pt and Ir may be appropriate from this standpoint. For industrial operations, however, affordable materials could be required as substitutes for these expensive noble metal anodes. Chromium-based alloys are reported [28] as one of the candidates satisfying depletion resistance and affordability. The anode material shows stable behaviour at 1565°C due to the

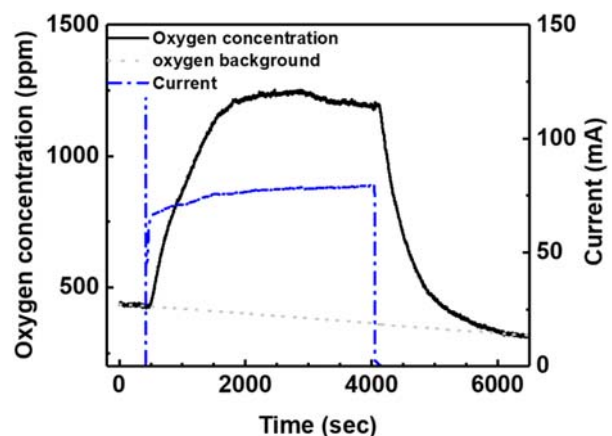


Figure 10. Current (dashed-dotted line) and oxygen concentration of outlet gas (solid line) during electrolysis with an Pt cathode and Pt coil anode at cell voltage of 2 V.

Table 4. Current efficiencies and energy consumptions at each electrolysis condition.

Electrolysis conditions	Current efficiency (avg. ± std. (%))	Energy consumption (avg. ± std. (kW h kg ⁻¹ of Fe))
1.4 V, 318 C	32.2 (±2.9)	6.11 (±0.51)
2 V, 318 C	54.7 (±2.4)	5.27 (±0.23)

corundum structure of a solid solution of chromium(III) and aluminium oxides which is also electronically conductive. Nickel and its alloy anodes are also used to evolve oxygen gas in the reports using hydroxide [6] and carbonates [7] electrolytes, but nickel oxides formed on the nickel anode can dissolve into molten oxide electrolytes. That is, the following properties are required for the potential anode materials: the low solubility of oxides formed on the anode to oxide electrolyte, and electronically conductivity of the oxide layer. It is expected that other candidates for affordable anode materials would be developed taking an advantage of the low process temperature of the present study.

Conclusion

In this paper, Fe_2O_3 was reduced using a molten $\text{B}_2\text{O}_3\text{-Na}_2\text{O}$ electrolyte with oxygen gas evolving as a by-product. The reduction of ferric ion occurred in a two-step reaction: the reduction from Fe^{3+} to Fe^{2+} is followed by the reduction from Fe^{2+} to Fe. A Pt-Fe alloy was formed on the surface of the Pt cathode at the potential less cathodic than the potential that Fe is reduced. The cathodic current efficiency increased as the cell voltage increased from 1.4 V to 2 V. This can be attributed to a decrease in the ratio of electronic current to total current. The average energy consumption was $5.27 \text{ kW h } 1 \text{ kg}^{-1}$ of Fe at 2-V electrolysis at 1000°C low for an oxide melt. Therefore, the $\text{B}_2\text{O}_3\text{-Na}_2\text{O}$ oxide system is promising as a supporting electrolyte to electrochemically reduce Fe_2O_3 to Fe without consuming any carbon.

Disclosure statement

No potential conflict of interest was reported by the author(s).

Funding

This work was supported by the POSCO [Grant number 0642-20190003].

ORCID

Ki Tae Nam  <http://orcid.org/0000-0001-6353-8877>
Kyung-Woo Yi  <http://orcid.org/0000-0002-7926-9541>

References

- [1] World Steel Association. World steel in figures. Brussels: World Steel Association; 2018.
- [2] Quader MA, Ahmed S, Dawal S, et al. Present needs, recent progress and future trends of energy-efficient ultra-low carbon dioxide (CO_2) steelmaking (ULCOS) program. *Renew Sustain Energy Rev.* 2016;55:537–549.
- [3] Meijer K, Denys M, Lasar J, et al. ULCOS: ultra-low CO_2 steelmaking. *Ironmak Steelmak.* 2009;36(4):249–251.
- [4] Croezen H, Korteland M. Technological developments in Europe, Delft; 2010.
- [5] Allanore A, Lavelaine H, Valentin G, et al. Electrodeposition of metal iron from dissolved species in alkaline media. *J Electrochem Soc.* 2007;154(12):E187–E193.
- [6] Cox A, Fray D. Electrolytic formation of iron from haematite in molten sodium hydroxide. *Ironmak Steelmak.* 2008;35(8):561–566.
- [7] Yin H, Tang D, Zhu H, et al. Production of iron and oxygen in molten $\text{K}_2\text{CO}_3\text{-Na}_2\text{CO}_3$ by electrochemically splitting Fe_2O_3 using a cost affordable inert anode. *Electrochem Commun.* 2011;13(12):1521–1524.
- [8] Li H, Jia L, Liang J-I, et al. Study on the direct electrochemical reduction of Fe_2O_3 in NaCl-CaCl_2 melt. *Int J Electrochem Sci.* 2019;14(12):11267–11278.
- [9] Wang D, Gmitter AJ, Sadoway DR. Production of oxygen gas and liquid metal by electrochemical decomposition of molten iron oxide. *J Electrochem Soc.* 2011;158(6):E51–E54.
- [10] Kim H, Paramore J, Allanore A, et al. Electrolysis of molten iron oxide with an iridium anode: the role of electrolyte basicity. *J Electrochem Soc.* 2011;158(10):E101–E105.
- [11] Liu J-H, Zhang G-H, Chou K-C. Electrolysis of molten FeO_x -containing $\text{CaO-Al}_2\text{O}_3\text{-SiO}_2$ slags under constant current field. *J Electrochem Soc.* 2015;162(12):E314–E318.
- [12] Zhang K, Jiao H, Zhou Z, et al. Electrochemical behavior of Fe (III) ion in $\text{CaO-MgO-SiO}_2\text{-Al}_2\text{O}_3\text{-NaF-Fe}_2\text{O}_3$ melts at 1673 K. *J Electrochem Soc.* 2016;163(13):D710–D714.
- [13] Allanore A. Electrochemical engineering for commodity metals extraction. *Electrochem Soc Interface.* 2017;26(2):63–68.
- [14] Allanore A. Features and challenges of molten oxide electrolytes for metal extraction. *J Electrochem Soc.* 2015;162(1):E13–E22.
- [15] Allanore A, Sadoway DR. US Patent No. 8764962 B2; 2014.
- [16] Allanore A. Electrochemical engineering of anodic oxygen evolution in molten oxides. *Electrochim Acta.* 2013;110:587–592.
- [17] Duffy JA. A review of optical basicity and its applications to oxidic systems. *Geochim Cosmochim Acta.* 1993;57(16):3961–3970.
- [18] Barati M, Coley KS. Electrical and electronic conductivity of $\text{CaO-SiO}_2\text{-FeOx}$ slags at various oxygen potentials: Part I. experimental results. *Metall Mater Trans B.* 2006;37(1):41–49.
- [19] Shartsis L, Capps W, Spinner S. Density and expansivity of alkali borates and density characteristics of some other binary glasses. *J Am Ceram Soc.* 1953;36(2):35–43.
- [20] Shartsis L, Capps W, Spinner S. Viscosity and electrical resistivity of molten alkali borates. *J Am Ceram Soc.* 1953;36(10):319–326.
- [21] Bale CW, Bélisle E, Chartrand P, et al. Reprint of: factSage thermochemical software and databases, 2010–2016. *Calphad.* 2016;55:1–19.
- [22] Fredriksson P, Sundman B. A thermodynamic assessment of the Fe–Pt system. *Calphad.* 2001;25(4):535–548.
- [23] Mamantov G, Manning D, Dale J. Reversible deposition of metals on solid electrodes by voltammetry with linearly varying potential. *J Electroanal Chem.* 1965;9(4):253–259.
- [24] Takahashi K, Miura Y. Electrochemical studies on diffusion and redox behavior of various metal ions in some molten glasses. *J Non-Cryst Solids.* 1980;38–39:527–532.
- [25] Popov K, Grgur B, Djokić SS. Fundamental aspects of electrometallurgy. New York: Springer; 2007.
- [26] Barati M, Coley KS. Electrical and electronic conductivity of $\text{CaO-SiO}_2\text{-FeOx}$ slags at various oxygen potentials: Part II. Mechanism and a model of electronic conduction. *Metall Mater Trans B.* 2006;37(1):51–60.
- [27] Wiencke J, Lavelaine H, Panteix P-J, et al. Electrolysis of iron in a molten oxide electrolyte. *J Appl Electrochem.* 2018;48(1):115–126.
- [28] Allanore A, Yin L, Sadoway DR. A new anode material for oxygen evolution in molten oxide electrolysis. *Nature.* 2013;497:353–356.